2018

Non-vacuum Preparation of wse2 Thin Films via the Selenization of Hydrated Tungsten Oxide Prepared using Chemical Solution Methods

Christopher L. Exstrom

Scott A. Darveau

Megan E. Flaconer

Jessica R. Blum

Whitney M. Colling

See next page for additional authors

Authors

Christopher L. Exstrom, Scott A. Darveau, Megan E. Flaconer, Jessica R. Blum, Whitney M. Colling, and Natale J. Ianno

MRS Advances © 2018 Materials Research Society
DOI: 10.1557/adv.2018.451

Non-vacuum Preparation of wse_2 Thin Films *via* the Selenization of Hydrated Tungsten Oxide Prepared using Chemical Solution Methods

Christopher L. Exstrom[1], Scott A. Darveau[1], Megan E. Falconer[1], Jessica R. Blum[1], Whitney M. Colling[1], and Natale J. Ianno[2]

[1]*Department of Chemistry, University of Nebraska at Kearney, Kearney, NE 68849-1150, U.S.A.*

[2]*Department of Electrical & Computer Engineering, University of Nebraska-Lincoln, Lincoln, NE 68588-0511, U.S.A.*

ABSTRACT

It is known that tungsten oxide may be reacted with selenium sources to form WSe_2 but literature reports include processing steps that involve high temperatures, reducing atmospheres, and/or oxidative pre-treatments of tungsten oxide. In this work, we report a non-vacuum process for the fabrication of compositionally high quality WSe_2 thin films via the selenization of tungsten oxide under milder conditions. Tungsten source materials were various hydrated WO_3 and $WO_{2.9}$ compounds that were prepared using chemical solution techniques. Resulting films were selenized using a two-stage heating profile (250 ^oC for 15 minutes and 550 ^oC for 30 minutes) under a static argon atmosphere. Effects of the starting tungsten oxide phase on WSe_2 formation after single and double selenization cycles were investigated using Raman spectroscopy and X-ray diffraction (XRD). After two selenization cycles, hydrated WO_3 was converted to (002)-oriented WSe_2 that exhibits well-resolved peaks for E^1_{2g} and A_{1g} phonon modes. Only a single selenization cycle was required to convert amorphous $WO_{2.9}$ to WSe_2. All selenizations in this work were achieved in non-reducing atmospheres and at lower temperatures and shorter times than any non-laser-assisted processes reported for WO_3-to-WSe_2 conversions.

INTRODUCTION

With its low mineral extraction costs [1], a reported direct bandgap of 1.35-1.5 eV [2] and high minority carrier mobility [3], the WSe_2 material system is seeing renewed interest in next-generation solar cell absorber material development. Heterojunction photovoltaic (PV) devices based on WSe_2 single-crystal absorbers have had reported efficiencies exceeding 8% [4]. Fabrication of WSe_2 films *via* the selenization of tungsten has been shown to be effective at temperatures > 900 ^oC and reaction times longer than 24 hrs [5] due to a large activation energy barrier that accompanies the lattice expansion. So-called "soft selenization" of tungsten [3,6] at temperatures of 450-560 ^oC over 24 hrs has yielded WSe_2 films of non-specific orientation and there is no evidence for electronic properties that would be suitable for

PV applications. More recently, a laser-assisted selenization method has been successfully executed at 250 ^{o}C, but this is useful only in conjunction with small-spot targeting [7].

It is known that tungsten oxide may be reacted with various selenium sources to form WSe_2 but literature reports still include processing steps that involve high temperatures and/or reducing atmospheres [8-14]. Selenization temperatures of evaporated WO_3 films have been reduced from 950 to 800 ^{o}C after the inclusion of a Ni backlayer that forms one or more relatively low-temperature melting $NiSe_{2-x}$ phases which act as intermediates in WSe_2 formation [15]. Selenization of native WO_3 films on tungsten have been reported at 650 ^{o}C in a reducing atmosphere [16]. It has been proposed that the initial step in this mechanism is the reaction between H_2 and WO_3 to produce oxygen-deficient WO_{3-x} species that undergo thermodynamically favorable substitutions of oxygen by selenium.

We have discovered that the nature of the WO_3 precursor film can significantly affect the minimum time and temperature requirements for selenization. In this report, we describe the results of selenization of various WO_3 and $WO_{2.9}$ compounds prepared using chemical solution methods. Heating these films in the presence of excess Se in a non-reducing argon atmosphere at temperatures no higher than 550 ^{o}C for heating/dwelling/cooling times totaling no more than 3 hours results in partial or complete conversion to WSe_2. No dynamic vacuum, inert gas flow, or higher-temperature post-anneal is required. Raman spectra and XRD patterns consistent with those for films prepared by higher-temperature and longer-time selenization of evaporated WO_3 films.

EXPERIMENT

Hydrated WO_3 (HTO) preparation [17]

A solution of 3 mL diethyl sulfate (Aldrich, 98%), 87 mL deionized water and 1.65, 2.15 or 2.50 g of $Na_2WO_4 \cdot 2H_2O$ (Mallinckrot) was prepared, heated to 90 ^{o}C with stirring and held at that temperature for five minutes. The resulting yellow or yellow-white particle suspension was transferred to a 50-mL centrifuge tube containing a 1-inch diameter Corning 1737F glass disk at the bottom. Particle deposition was achieved through centrifugation [18] at 2000g for eight minutes. The resulting yellow-white films were visibly particulate and scratched easily, so thickness measurements were not possible.

$WO_{2.9}$ (blue tungsten oxide or BTO) preparation [19].

A dip-coating solution was prepared by combining 2 g WCl_6 (Aldrich, 99.9%) and 20 mL anhydrous ethanol (Pharmco-Aaper) and the resulting blue solution was stirred for several hours prior to dip coating (12.5 mm/s speed) onto 1-inch Corning 1737F glass disks. The resulting blue films were visibly smooth and translucent but scratched easily, so thickness measurements were not possible.

Selenization and film characterization.

Coated substrates were placed in a graphite susceptor containing excess Se and heated under an argon atmosphere. The sample temperature was increased by 25 ^{o}C/min to 250 ^{o}C and held there for 15 minutes. This was followed by another 25 ^{o}C/min ramp to 550 ^{o}C where, unless otherwise specified, the sample dwelled for 30 minutes then cooled to room temperature over 1 hour. This entire process will be referred to as a

selenization "cycle". After characterization by Raman spectroscopy and x-ray diffraction (XRD), the film was subjected to a second identical selenization cycle unless otherwise specified. Some degree of flaking and thickness inhomogeneities were observed in the gray product films, which scratched easily upon attempts to remove samples for electron microscopy analysis.

RESULTS AND DISCUSSION

Three samples of HTO materials were prepared by varying the initial solution $Na_2WO_4 \cdot 2H_2O$ concentrations (0.0538, 0.0701, 0.0815 M). No steps were taken to buffer pH levels which were initially 8.34, 8.63, and 8.79, respectively, and decreased by approximately 2 units during the heating and HTO formation processes due to H_3O^+ release by diethyl sulfate [20]. Raman spectra (Figure 1, left) of these samples show peaks in the 600-850 cm^{-1} region due to O-W-O bending modes and a peak at 950 cm^{-1} from surface W=O bond stretching [21]. This last peak is most intense in the 0.0538 M sample and the general spectral shape is consistent with the dihydrate form of WO_3. As the sodium tungstate concentration was increased, this peak diminished in intensity and the lower O-W-O bending frequency shift higher to match what has been reported for the monohydrate WO_3 form [21]. The XRD pattern (Figure 1, right) of the 0.0701 M sample indicates that it consists mainly of hexagonal $WO_3 \cdot 1/3H_2O$ [22] while the other HTO sample patterns do not match well with any in single-phase JCPDS cards. The 0.0701 and 0.0815 M samples exhibit intense peaks at $2\theta = 10.49^o$ and 10.65^o, respectively. These are consistent with reported reflections from oxygen-deficient species such as m-$W_{18}O_{49}$ (200) [23] and $H_{12}W_{12}O_{42} \cdot 21H_2O$ (111) [24]. The formation of the latter compound would be consistent with a previously proposed mechanism for this reaction [20]. Using Scherrer's formula [25], crystallite sizes were estimated to be 45-60, 25-50, and 65-90 nm for the 0.0538, 0.0701, 0.0815 M samples, respectively.

The reaction of WCl_6 and anhydrous ethanol results in the formation of a deep blue solution consisting of $WO_{2.9}$ (BTO) [19]. This oxygen deficiency results in the partial reduction of tungsten and creates a low-energy W^{5+}-to-W^{6+} intervalence charge transfer transition leading to the blue color [26]. After dip-coating, the resulting sample

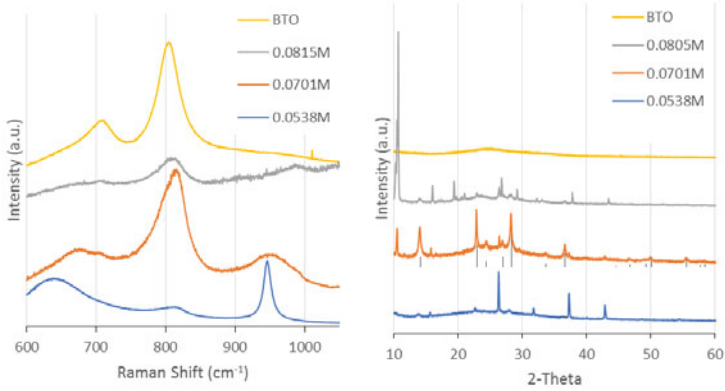

Figure 1. Raman spectra (left) and XRD patterns (right) of as-made BTO films and HTO films prepared from 0.0815, 0.0701, and 0.0538 M Na_2WO_4 solutions, respectively. Legend orders match the spectrum/pattern orders top-to-bottom. The vertical lines under the 0.0701 M XRD pattern are from JCPDS card no. 35-1001 for hexagonal $WO_3 \cdot 1/3\ H_2O$.

exhibited no significant XRD peaks and only O-W-O bending modes (710, 806 cm^{-1}) were present in the Raman spectrum (Figure 1, left).

Each sample was selenized under identical conditions as described in the Experiment section. After one selenization cycle, the 0.0538 M sample was partially converted to WSe_2. The XRD pattern (Figure 2) exhibits prominent peaks assigned to the 002, 006, and 008 WSe_2 reflections; however, noticeable peaks at $2\theta = 16.5^o$ and 24-30^o due to orthorhombic and monoclinic WO_3, respectively, are also present. The Raman spectrum (Figure 3), reveals the presence of WSe_2 with distinguishable E^1_{2g} and A_{1g} mode peaks at 250 and 255 cm^{-1}. Spectral separation of these modes has been linked to mobility carrier properties that are promising for photovoltaic applications [27].

After a second selenization cycle, the WO_3 (Raman, XRD) and Se (Raman) peaks were no longer present and the WSe_2 E^1_{2g} and A_{1g} mode peaks were shifted to 248 and 252 cm^{-1}, respectively. These are consistent with frequencies reported for WSe_2 thin films and the shift indicates the relief of lattice strain during the second selenization cycle [10]. Peaks stemming from A_{1g}-LA modes [28] at 371 and 393 cm^{-1} are much more prominent.

Selenization (one cycle) of the 0.0701 M sample results in a Raman spectrum (Figure 3) that shows only WSe_2 peaks with the possible exception of a small peak at 910 cm^{-1} that could be due to W=O stretching from residual WO_3 that is also apparent from XRD peaks (Figure 2) at $2\theta = 24.16^o$ and 28.33^o (m-WO_3). The most prominent XRD

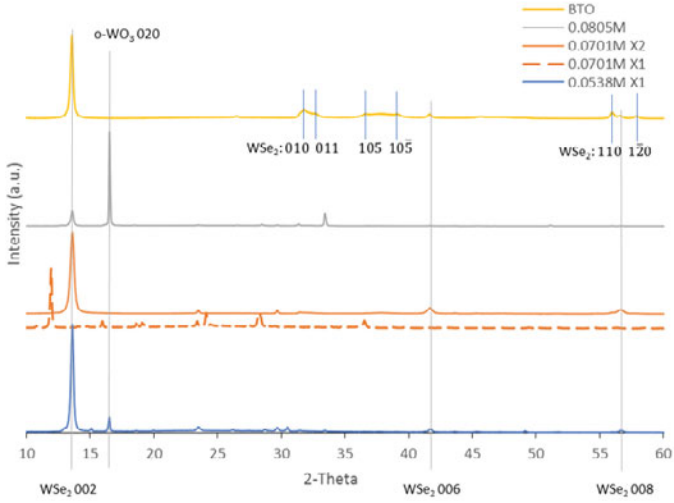

Figure 2. XRD patterns of selenized BTO films and HTO films prepared from 0.0815, 0.0701, and 0.0538 M Na_2WO_4 solutions, respectively. Legend orders match the spectrum order top-to-bottom. 1X = one selenization cycle, 2X = two selenization cycles.

peak is at $2\theta = 11.94^o$. While this angle does not match those for any reported WSe_2 reflections [29], it is possible that unit cell compression shifted the 002 peak from its typical $2\theta = 13.7^o$ angle. After a second selenization cycle, a well-oriented WSe_2 results as indicated by prominent 002 ($2\theta = 13.77^o$), 006 (41.56^o), and 008 (56.44^o) reflections at expected angles. The Raman spectrum shows slight red shifts of the E^1_{2g} and A_{1g} phonon

mode frequencies by 1-2 cm^{-1}. Interestingly, doubling the 550 ^{o}C dwell time during the first selenization does not remove the residual WO_3 from the sample that was observed after one of our standard selenization cycles. It is possible that the cooldown step between the first and second selenization cycles induces the crystallization of a strained WSe_2 lattice, perhaps due to incomplete oxygen displacement or the presence of residual WO_3, that is more reactive to further selenization. Further investigation is in process.

After one selenization cycle, the 0.0815 M sample exhibited Raman peaks (Figure 3) due to WSe_2 (E^1_{2g}/A_{1g} modes at 247 cm^{-1}) and WO_3 (O-W-O bending at 765 cm^{-1} and W=O stretching at 944 cm^{-1}). The XRD pattern (Figure 2) shows prominent peaks from WSe_2 002 (2θ = 13.61^{o}) and 011 (33.43^{o}) as well as the (020) reflection (16.54^{o}) from o-WO_3. A second selenization does not affect these spectra.

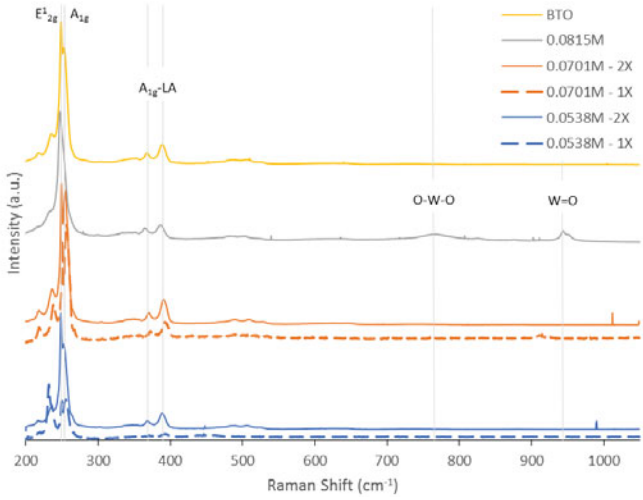

Figure 3. Raman spectra of selenized BTO films and HTO films prepared from 0.0815, 0.0701, and 0.0538 M Na_2WO_4 solutions, respectively. Legend orders match the spectrum order top-to-bottom. 1X = one selenization cycle, 2X = two selenization cycles.

A single selenization of the BTO film results in XRD and Raman peaks that can all be assigned to WSe_2. In the XRD pattern (Figure 2), the (002) reflection is the most prominent but the presence of several non-c-axis-oriented reflection plane peaks indicates that the film is not as well-oriented as the double-selenized 0.0538 and 0.0701 M HTO samples. The Raman spectrum (Figure 3) does feature distinguishable E^1_{2g} and A_{1g} mode peaks at 248 and 252 cm^{-1}.

All selenizations in this work were achieved in non-reducing atmospheres and at lower temperatures and shorter times than any non-laser-assisted processes reported for WO_3-to-WSe_2 conversions. Thermodynamically, selenization of WO_x in non-reducing atmospheres becomes favorable when $x < 2$ [16]. While there is no evidence of such species present during these reactions, our observations may lend insight about kinetic factors that could lower activation energies. Access of selenium vapor to tungsten atoms in the crystal lattice may be important. This may be facilitated by the particulate and somewhat porous nature of our films. However, hydration of WO_3 structures opens spaces between planes of tungsten coordination units in the crystal

lattice [21]. There is also the possibility of Se reacting with these waters of hydration to form trace quantities of H_2Se that may act as an intermediate in the selenization mechanism [10]. In the case of $WO_{2.9}$ selenization, a greater number of oxygen-deficient WO_x sites may lead to faster reactivity, possibly through defect-induced partial encapulsation mechanisms [30].

ACKNOWLEDGMENT

This work was funded by the University of Nebraska Foundation.

REFERENCES

1. C.Wadia, A.P. Alivastos, and D.M. Kammen, Environ. Sci. Technol. **43**, 2072 (2009).
2. A. Jäger-Waldau, M. Ch. Lux-Steiner, and E. Bucher, Solid State Phen. **37-38**, 479 (1994).
3. A. Jäger-Waldau, and E. Bucher, Thin Solid Films **200**, 157 (1991).
4. M. Vogt, M. Ch. Lux-Steiner, P. Dolatzoglou, and E. Bucher, presented at the 1988 Photovoltaic Solar Energy Conference, Florence, Italy (unpublished).
5. Q. Ma, H. Kyureghian, J.D. Banninga, and N.J. Ianno, Mater. Res. Soc. Symp. Proc. **1670**, San Francisco, CA, 2014, mrss14-1670-e01-02 doi:10.1557/opl.2014.739.
6. J. Pouzet, J. C. Bernede, A. Khellil, H. Essaidi, S. Benhida, Thin Solid Films **208**, 259 (1992).
7. Y.-Z. Chen, H. Medina, T.-Y. Su, J.-G. Li, K.-Y. Cheng, P.-W. Chiu, and Y.-L. Chueh, ACS Nano **9**, 4346 (2015)
8. P.M. Campbell, A. Tarasov, C.A. Joiner, M.-Y. Tsai, G. Pavlidis, S. Graham, W.J. Ready, and E.M. Vogel, Nanoscale **8**, 2268 (2006).
9. J.-K. Huang, J. Pu, C.-L. Hsu, M.-H. Chiu, Z.-Y. Juang, Y.-H. Chang, W.-H. Chang, Y. Iwasa, T. Takenobu, and L.-J. Li, ACS Nano **8**, 923 (2014).
10. K. Xu, F. Wang, Z.Wang, X. Zhan, Q. Wang, Z. Cheng, M. Safdar, and J. He, ACS Nano **8**, 8468 (2014).
11. P. Browning, S. Eichfeld, K. Zhang, L. Hossain, Y.-C. Lin, K. Wang, N. Lu, A.R. Waite, A.A. Voevodin, M. Kim, and J. Robinson, 2D Mater. **2**, 014003 (2015)
12. J. Chen, W. Zhou, W. Tang, B. Tian, X. Zhao, H. Xu, Y. Liu, D. Geng, S.J.R. Tan, W. Fu, and K.P. Loh, Chem. Mater. **28**, 7194 (2016).
13. F. Ullah, Y. Sim, C.T. Le, M.-J. Seong, J.I. Jang, S.H. Rhim, B.C.T. Khac, K.-H. Chung, K. Park, Y. Lee, K. Kim, H.Y. Jeong, and Y.S. Kim, ACS Nano **11**, 8822 (2017).
14. Y. Lee, H. Jeong, Y.-S. Park, S. Han, J. Noh, and J.S. Lee, Appl. Surf. Sci. **432**, 170 (2018).
15. G. Salitra, G. Hodes, E. Klein, and R. Tenne, Thin Solid Films **245**, 180 (1994).
16. H. Kim, S.J. Yun, J.C. Park, M.H. Park, J.-H. Park, K.K. Kim, and Y.H. Lee, Small **11**, 2192 (2015).
17. M.Z. Najdoski and T. Todorovski, Mater. Chem. Phys. **104**, 483 (2007).
18. A.R. Markelonis, J.S. Wang, B. Ullrich, C.M. Wai, G.J. Brown, Appl. Nanosci. **5**, 457 (2015).
19. W. Cheng, E. Baudrin, B. Dunn, and J. Zink, J. Mater. Chem. **11**, 92 (2001).
20. R.R. Kharade, S.R. Mane, R.M. Mane, P.S. Patil, P.N. Bhosale, J Sol-Gel Sci. Technol. **56**, 177 (2010).
21. A.K. Nayak, S. Lee, Y.I. Choi, H.J. Yoon, Y. Sohn, and D. Pradhan, ACS Sustainable Chem. Eng. **5**, 2741 (2017).
22. JCPDS card no. 35-1001.
23. A. Karuppasamy, Appl. Surf. Sci. **282**, 77 (2013).
24. Z.-F. Li, B.-S. Zhang, Z. Kristallographie **223**, 191 (2008).
25. A.L. Patterson, Phys. Rev. **56**, 978 (1939).
26. O.J. Klejnot, Inorg. Chem. **4**, 1668 (1965).
27. P. Tonndorf, R. Schmidt, P. Böttger, X. Zhang, J. Börner, A. Liebig, M. Albrecht, C. Kloc, O. Gordau, D.R.T. Zahn, S.M. de Vasconcellos, R. Bratschitsch, Optics Express **21**, 4908 (2013).
28. D.J. Late, S.N. Shirodkar, U.V. Waghmare, V.P. Dravid, and C.N.R. Rao, ChemPhysChem 15, 1592 (2014).
29. W.J. Schutte, J.L. de Boer, F. Jellinek, J. Solid State Chem. **70**, 207 (1987).
30. J. Sloan, J.L. Hutchison, R. Tenne, Y. Feldman, T. Tsirlina, and M. Homyonfer, J. Solid State Chem. **144**, 100 (1999).